Progress In Electromagnetics Research, Vol. 144, 261–270, 2014

Two-Dimensional Microwave Tomographic Algorithm for Radar Imaging through Multilayered Media

Wenji Zhang*

Abstract—The imaging of targets embedded in a planar layered background media has been an important topic in subsurface and urban sensing. In this paper a fast and efficient tomographic algorithm for the imaging of targets embedded in a multilayered media is presented. The imaging algorithm is based on the first-order Born approximation and exploits the spectral multilayered media Green's function. The exploding reflection model is employed and then the Green's function is expanded in the spectral form to facilitate the easy implementation of the imaging algorithm with fast Fourier transform (FFT). The wave propagation effect due to the presence of the layered subsurface media is automatically taken into account in the imaging formulation through the multilayer media Green's function. The linearization of the inversion scheme and employment of FFT make the imaging algorithm suitable in several applications concerning the diagnostics of large probed domain and allow real-time processing. Representative examples are presented to show the effectiveness and efficiency of the proposed algorithm for radar imaging through multilayered media.

1. INTRODUCTION

Ground penetrating radar (GPR) has been broadly used in many civilian and military applications in order to nondestructively investigate the subsurface property, i.e., in geological and archeological surveys, for detecting buried objects and locating subsurface cavities, due to its easy usage, quick operation, and low cost [1–8]. It is less destructive and can provide more information than other methods of exploration, i.e., borehole and drilling radar systems. These advantages have sparked a growing interest in GPR imaging algorithms for subsurface nondestructive testing.

During the past decade, several effective subsurface imaging algorithms have been developed to reconstruct targets buried under ground. In [9–11] the reconstruction of the target permittivity distribution is cast as the minimization of a non-quadratic cost function and solved with global or deterministic optimization methods. To improve the computation efficiency, the distorted Born iterative method (DBIM) and Born iterative method (BIM) dealing with intermediate scatterers are developed in [12, 13]. BIM and DBIM start with the first-order Born inversion result and are solved iteratively by incrementally correcting the estimated contrast function in every iteration step. Subsurface imaging algorithms should be computationally efficient, so that the location of the buried objects can be determined in a few seconds for on-site measurement. For a typical GPR survey, this requirement prohibits the use of iterative, nonlinear inversion schemes. In order to reduce the requirement of computation resources and make the imaging algorithm suitable for on-site applications, linear simplifications or approximations of the scattering process are usually employed [2, 14]. Under the ideal point target model, subsurface beamforming algorithms using ray tracing technique are proposed in [14–17]. In these algorithms ray tracing technique is used to calculate the wave propagation time from the radar in the air to the target buried under ground. Due to the highly simplified assumptions of wave propagation phenomenon, the only part of the information contained in the GPR signal that is

Received 3 September 2013, Accepted 13 January 2014, Scheduled 29 January 2014
* Corresponding author: Wenji Zhang (wenjizhang@gmail.com).
The author is with the Department of Electrical and Computer Engineering, Duke University Durham, NC 27708, USA.

exploited in the imaging algorithm is the propagation time. Moreover, a nonlinear equation has to be solved in order to find the wave propagation path using ray tracing technique which is time consuming and difficult to be extended to complex subsurface environment involving layered soils. As an efficient compromise between the imaging accuracy and efficiency, tomographic imaging algorithms based on the first order Born or Rytov approximation are proposed in [18–20]. Tomographic imaging algorithms provide efficient quantitative reconstruction of cross-sections of inhomogeneous objects, such as their location, shape and electrical properties, etc. [18–25].

Most of the aforementioned subsurface imaging algorithms mainly deal with a two layered homogeneous media, in which the upper region is the air and the lower region is the homogeneous soil. During the past decade, imaging of inhomogeneous objects embedded in a planar layered background media has attracted growing interest. A layered media represents a more realistic model than a homogeneous single layer half space background. It is of practical importance and interest to extend the GPR imaging to buried targets under multilayered subsurface media. Due to the limitation of the computation complexity of ray tracing technique, it is very difficult to generalize the ray tracing based backprojection algorithm to multilayered media. A linear inverse scattering algorithm for the imaging of 2D objects buried in a two-layered media was proposed in [25]. A piecewise and Wiener filter-based SAR techniques are presented for the imaging of targets in layered structures in [23]. Nonlinear iterative imaging algorithm for the reconstruction of concealed targets buried in a multilayered media environment was proposed in [29]. The computation time increases significantly with the increasing of number of pixels in the image, making the iterative algorithms very difficult to be used for on-site applications. In this paper a fast and efficient tomographic algorithm for the imaging of inhomogeneous objects embedded in a planar multilayered subsurface media is presented. The imaging algorithm is based on the first-order Born approximation and employing the multilayered media Green's function. The exploding reflection model is employed and then the Green's function is expanded in the spectral domain to facilitate the implementation of the imaging algorithm with fast Fourier transform (FFT). The linearization of the inversion scheme and the employment of FFT in the imaging formula make it suitable for several applications concerning the diagnostics of large probed region and allow real-time processing.

The organization of the remainder of the paper is as follows. In Section 2, the formulation of the real-time subsurface tomography algorithm for the imaging of targets buried under a planar multilayered media is presented. Numerical results are presented in Section 3 to show the effectiveness of the proposed algorithm. Finally, some conclusions are drawn in Section 4.

2. FORMULATION OF THE PROBLEM

Figure 1 shows a typical scenario of ground penetrating synthetic aperture radar imaging through multilayered media. We consider a multilayer plane structure formed by N lossy homogeneous layers. The stratified layers of the background media are characterized by material electrical parameters ε_1, μ_1;

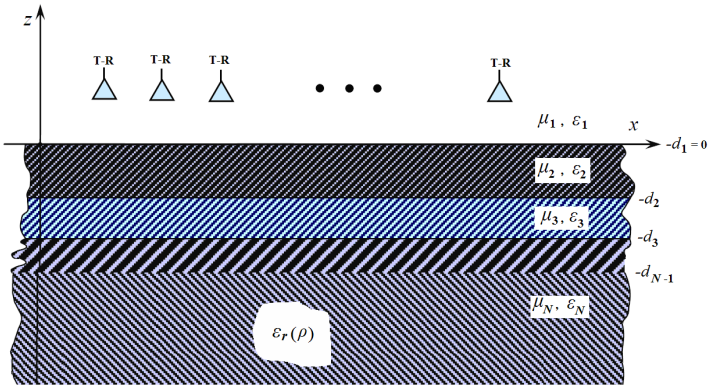

Figure 1. Geometrical configuration of GPR imaging through multilayered media.

ε_2, μ_2; ...; ε_i, μ_i; ...; ε_N, μ_N for the 1, 2, ..., i, ..., Nth layer. Permeabilities μ_1, μ_2, ..., μ_N are equal to the magnetic constant of a vacuum μ_0. Permittivities ε_1, ε_2, ..., ε_N may take complex values. In this paper we consider the two-dimensional (2-D) problem in which the layered media and target are assumed to be infinitely long and invariant along the y-axis. The monostatic radar system transmits electromagnetic wave along a scan line above the ground from $-x_s$ to x_s and collects echoes. The scan line, denoted as D_{obs} is parallel to the x-axis at a height $z = z_R > 0$. The working frequency of the radar system ranges from $f_{\min}$ to $f_{\max}$ with frequency step Δf. The targets to be imaged are located in an inaccessible investigated region denoted as D_{inv} in Region N. The investigated domain is chosen to be a rectangular region ranging from $-x_{inv}$ to x_{inv} and $z_{\min}$ to $z_{\max}$ in layer N. The relative complex permittivity $\varepsilon_r(\boldsymbol{\rho})$ inside D_{inv} can be defined as

$$\varepsilon_r(\boldsymbol{\rho}) = \begin{cases} \varepsilon_{ri}(\boldsymbol{\rho}), & \boldsymbol{\rho} \in D_{inv} \\ \varepsilon_N, & \text{otherwise} \end{cases} \tag{1}$$

where $\boldsymbol{\rho} = \hat{x}x + \hat{z}z$ is a spatial vector.

Assume that the electric current is a 2-D point source, which is equivalent to a 3-D line source directed in the y direction. In this case only the y component of the electric field is nonzero and hence the subscript y will be omitted in the following formulations. Then, the scattered electric field from 2-D buried targets at the receiver can be written as

$$E_s(\boldsymbol{\rho}_R, k) = k^2 \int_{D_{inv}} G(\boldsymbol{\rho}_R, \boldsymbol{\rho}, k)\, E_t(\boldsymbol{\rho}, \boldsymbol{\rho}_S, k)\, \chi(\boldsymbol{\rho}) d\boldsymbol{\rho} \tag{2}$$

where k is the wavenumber in the free space, $\boldsymbol{\rho}_R = \hat{x}x_R + \hat{z}z_R$ the position of the receiver, $\boldsymbol{\rho}_S = \hat{x}x_S + \hat{z}z_S$ the position of the transmitter, G the Green's function for the background layered media, $E_t(\boldsymbol{\rho}, \boldsymbol{\rho}_S, k)$ the total electrical field inside the target, $\chi(\boldsymbol{\rho})$ the contrast function of the object $\chi(\boldsymbol{\rho}) = \varepsilon_{ri}(\boldsymbol{\rho}) - \varepsilon_N$, ε_{ri} the relative permittivity of the object, and ε_N the relative permittivity of the N-th layer. The total field inside the target also depends on the contrast of the target. Thus (2) is a nonlinear equation that is very time consuming to solve. In order to linearize the equation and accelerate the imaging algorithm, the first-order Born approximation is employed, where the total field inside the target is approximated by the incident electric field

$$E_t(\boldsymbol{\rho}, \boldsymbol{\rho}_S, k) \cong E^{inc}(\boldsymbol{\rho}, \boldsymbol{\rho}_S, k) = ik\eta_0 G(\boldsymbol{\rho}, \boldsymbol{\rho}_S, k) \tag{3}$$

Then the received scattered field can be derived as

$$E_s(\boldsymbol{\rho}_R, k) = i\eta_0 k^3 \int_{D_{inv}} G(\boldsymbol{\rho}_R, \boldsymbol{\rho}, k)\, G(\boldsymbol{\rho}, \boldsymbol{\rho}_S, k)\, \chi(\boldsymbol{\rho})\, d\boldsymbol{\rho} \tag{4}$$

where η_0 is the wave impedance in the freespace. For the monostatic measurement configuration in which $\boldsymbol{\rho}_R = \boldsymbol{\rho}_S$, the received scattered field can be written as

$$E_s(\boldsymbol{\rho}_R, k) = i\eta_0 k^3 \int_{D_{inv}} G^2(\boldsymbol{\rho}_R, \boldsymbol{\rho}, k) \chi(\boldsymbol{\rho})\, d\boldsymbol{\rho} \tag{5}$$

In the above equation the reciprocity relationship has been used $G(\boldsymbol{\rho}_R, \boldsymbol{\rho}, k) = G(\boldsymbol{\rho}, \boldsymbol{\rho}_R, k)$.

The Green's function for the multilayered media can be expressed in the spectral form as [30]:

$$G(\boldsymbol{\rho}_R, \boldsymbol{\rho}, k) = \frac{i}{4\pi} \int_{-\infty}^{\infty} dk_x \frac{T(k_x)}{k_{1z}} \exp\left(ik_x(x_R - x) + ik_{1z}z_R - ik_{Nz}z\right) \tag{6}$$

where T is the transmission coefficient for the layered media.

For the multilayered homogeneous media shown in Figure 1, k_i is the wavenumber in the i-th layer. By applying the boundary condition at the interface of each layer, the generalized reflection coefficient can be derived as [30]:

$$\tilde{R}_{i,i+1} = \frac{R_{i,i+1} + \tilde{R}_{i+1,i+2} \exp\left(j2k_{i+1,z}(d_{i+1} - d_i)\right)}{1 + R_{i,i+1}\tilde{R}_{i+1,i+2} \exp\left(j2k_{i+1,z}(d_{i+1} - d_i)\right)} \tag{7}$$

where $\tilde{R}_{i,i+1}$ is the generalized/total reflection coefficient from the $i+1$th layer to the ith layer, k_{iz} the normal components of the propagation constant in the i-th layer, $-d_{i+1}$ the coordinate of the interface

between the $i+1$th and ith layers in z direction, and $R_{i,i+1}$ the reflection coefficient from the $i+1$th layer to the ith layer, i.e.,

$$R_{ij} = \frac{k_{iz} - k_{jz}}{k_{iz} + k_{jz}}, \quad T_{ij} = \frac{2k_{iz}}{k_{iz} + k_{jz}} \tag{8}$$

The generalized transmission coefficient from the first layer to the N-th layer can also be derived from the continuous boundary condition at the interface of each layer:

$$T_{1N} = \exp\left(-jk_{Nz}d_{N-1} + jk_{1z}d_1\right) \prod_{p=1}^{N-1} \exp\left(jk_{pz}\left(d_p - d_{p-1}\right)\right) S_{p,p+1} \tag{9}$$

where

$$S_{p-1,p} = \frac{T_{p-1,p}}{1 - R_{p-1,p}\tilde{R}_{p,p+1}\exp\left(j2k_{pz}\left(d_p - d_{p-1}\right)\right)} \tag{10}$$

and where $\tilde{R}_{p,p+1}$ can be calculated from (7).

For the convenience of derivation, (5) can be written in the following operator form

$$E_s\left(\boldsymbol{\rho}_R, k\right) = \left(L\chi\right)\left(\boldsymbol{\rho}\right) \tag{11}$$

The operator L maps the contrast function from the object space to the data space, in particular,

$$L(\cdot) \triangleq j\eta_0 k^3 \int_{D_{inv}} G^2(\boldsymbol{\rho}_R, \boldsymbol{\rho}, k)(\cdot)d\boldsymbol{\rho} \tag{12}$$

Then the image can be formulated by

$$I\left(r\right) = L^a\left(E_s\left(\boldsymbol{\rho}_R, k\right)\right) \tag{13}$$

where L^a is the adjoint operator of L and maps the scattered field from the data space to the object space, in particular [6, 31],

$$L^a(\cdot) \triangleq j\eta_0 \int_{k_{\min}}^{k_{\max}} dk k^3 \int_{D_{obs}} \left[G^2\left(\boldsymbol{\rho}_R, \boldsymbol{\rho}, k\right)\right]^* (\cdot)d\boldsymbol{\rho}_R \tag{14}$$

where $*$ denotes the conjugate operator. The complex conjugation in the adjoint operator is essentially the backpropagation of the wave to the location where it is excited. From the concept of time reversal imaging, the complex conjugation in the frequency domain is equivalent to the time reversal in the time domain. The backpropagation of the time reversed field will focus on the target. In the above equation the inner integrand corresponds to the beamforming over the cross range and the outer integrand is the coherent summation over all the operating frequencies.

In this paper, to obtain the real-time imaging algorithm the assumption of exploding reflection model is employed [35, 36]. In particular, $G^2(\boldsymbol{\rho}_R, \boldsymbol{\rho}, k)$ is replaced or approximated by $G(\boldsymbol{\rho}_R, \boldsymbol{\rho}, 2k)$. Then (14) can be further simplified as

$$L^a(\cdot) \triangleq -j\eta_0 \int_{k_{\min}}^{k_{\max}} dk k^3 \int_{D_{obs}} G^*(\boldsymbol{\rho}_R, \boldsymbol{\rho}, 2k)(\cdot)d\boldsymbol{\rho}_R \tag{15}$$

Substituting the spectral form of the Green's function (6) into (11) one has

$$L^a\left(E_s\left(r_R, k\right)\right) = \frac{-\eta_0}{4\pi} \int_{k_{\min}}^{k_{\max}} k^3 dk \int_{-\infty}^{\infty} dk_x T^*\left(k_x\right) \frac{\exp\left(ik_x x - ik_{1z}^* z_R + ik_{Nz}^* z\right)}{k_{1z}^*} \int_{D_{obs}} E_s\left(r_R, k\right) \exp\left(-ik_x x_R\right) dx_R \tag{16}$$

Due to employing of the exploding model $k_{iz} = \sqrt{4k_i^2 - k_x^2}$, $i = 1, 2, \ldots N$ in the above equation.

Then the image can be derived as

$$I\left(\boldsymbol{\rho}\right) = L^a\left(E_s\left(\boldsymbol{\rho}_R, k\right)\right) = \frac{-\eta_0}{4\pi} \int_{k_{\min}}^{k_{\max}} k^3 dk \int_{-\infty}^{\infty} dk_x \tilde{E}_s\left(k_x, k\right) T^*\left(k_x\right) \frac{\exp\left(ik_x x - ik_{1z}^* z_R + ik_{Nz}^* z\right)}{k_{1z}^*} \tag{17}$$

where $\tilde{E}_s(k_x, k)$ is the Fourier transform of $E_s(r_R, k)$ with respect to x_R, in particular

$$\tilde{E}_s\left(k_x, k\right) = \int_{D_{obs}} E_s\left(r_R, k\right) \exp\left(-ik_x x_R\right) dx_R \tag{18}$$

$\tilde{E}_s(k_x, k)$ can be calculated in a very short computation time by employing FFT. From the imaging formula one can find that:

(1) The complex scattering process due to presence of the multilayered background media is automatically included in the imaging formulation. The focusing delay due to the changes of the propagation speed and the bending effect of the wave in different layers has been taken into account through the Green's function.

(2) The time-consuming computation of the nonlinear equation aiming at finding the wave propagation path through different layers is avoided. The ray tracing technique employed in the conventional imaging algorithms in [14, 16, 17] becomes complicated and is generally difficult to solve for imaging of the target through multilayered media. However, the imaging algorithm proposed in this paper can deal with this problem very efficiently without noticeable increasing of computation time.

(3) The imaging process can be achieved in a short computation time by employing FFT, which is very welcome for real-time imaging applications.

3. NUMERICAL RESULTS

In order to show the effectiveness and efficiency of the proposed algorithm for radar imaging through multilayered media, some representative examples are presented in this section. In the following examples we assume that the permittivity and thickness of each layer are known. The inversion of multilayer media parameters is essentially a one-dimensional inverse scattering problem and has been well developed in the past two decades. We refer the readers to [32–34] for the estimation of parameters of multilayered media.

3.1. Imaging of Targets Embedded in a Single Layer Subsurface

In the first example, we investigate the imaging of two dielectric targets embedded in a single layer subsurface media, as shown in Figure 2(a). The forward scattered data were generated using Finite Difference Time Domain (FDTD) method, where the transmitter is an electrical dipole source. The monostatic radar measures the return signal at a distance of 0.3 m above the ground over a synthetic aperture extending from -2 m to 2 m with a step of 0.05 m. The permittivity and conductivity of the subsurface media are $\varepsilon_r = 6$ and $\sigma = 2$ mS/m. The operating frequency ranges from 1 GHz to 3 GHz with frequency step $\Delta f = 33.33$ MHz. The two targets investigated in this example from left to right in Figure 2(a) are a dielectric square and a dielectric rectangle with the designation of Target 1 and Target 2 respectively. The spatial characteristics of the targets are summarized in Table 1. The permittivity of the two objects is 10. The investigation domain is a 2 m $\times$ 1.6 m rectangular region and is divided into 150×120 pixels.

Figure 2(b) shows the imaging results of the targets using the proposed subsurface imaging algorithm. The true regions of the two targets are indicated with a white dashed square and rectangle. From this image it is found that the upper side of the object is correctly localized. However, the lower edges of the objects appear to be further than their true locations. This is due to the fact the Born approximation in the imaging algorithm assumes velocity of the electromagnetic waves equals to 12.25 cm/ns in the ground, while the actual velocity of the electromagnetic waves inside the object is 9.5 cm/ns. This leads the imaging algorithm to locate the lower edge further than its actual position. For comparison, the imaging results with the prestack migration algorithm in [14–16] are shown in Figure 2(c). From Figure 2(c) we find that prestack migration algorithm is also successful in imaging of the targets embedded in a single layer subsurface. Due to the point target model assumption in the prestack migration algorithm, which assumes the wave velocity inside the object to be the same as the background, we have similar observation that the lower edges of the dielectric object are localized further than their true locations. It takes about 33.67 s to form the image in Figure 2(c) using the prestack

Table 1. Target spatial characteristics.

	Target Type	**Size**	**Center Position**
Target 1	Rectangular	0.4 m $\times$ 0.3 m	(0.4 m, -1.0 m)
Target 2	Rectangular	0.3 m $\times$ 0.3 m	(-0.55 m, -1.2 m)

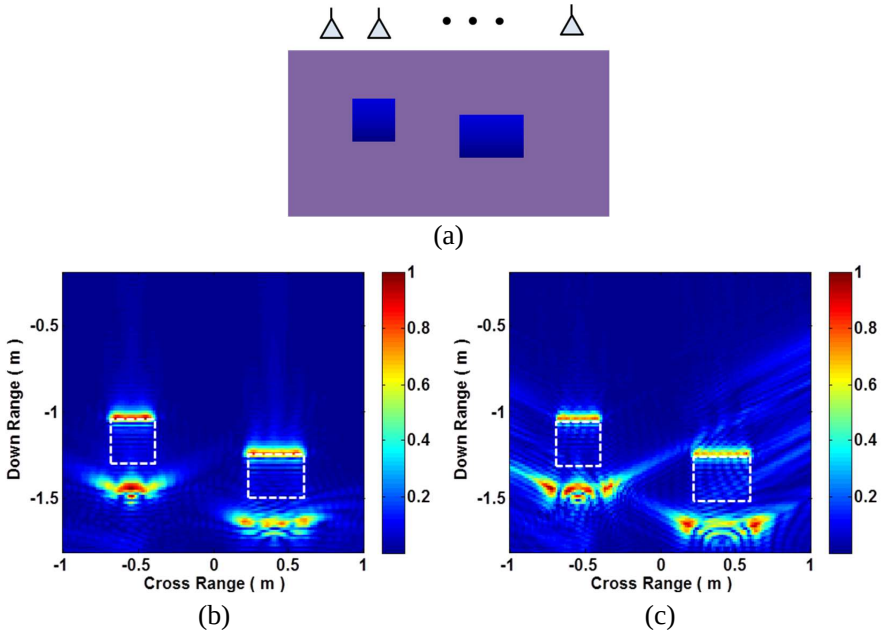

Figure 2. Imaging of targets buried under ground. (a) Simulation geometry. (b) Imaging result using the proposed algorithm. (c) Imaging result using the prestack migration algorithm.

migration algorithm on a 4-core P4 2.3 G, 4 G Ram personal computer. However, by using the proposed subsurface imaging algorithm, only 0.73 s is required to form the same size image in Figure 2(b). Due to the employment of FFT in the imaging algorithm, the imaging process can be achieved in a very short computation time, which is very useful for real time subsurface imaging.

3.2. Imaging of Targets under Multilayered Ground

In this example we present an imaging result of three targets buried under a two-layered media. The first layer is dry sand with dielectric constant $\varepsilon_r = 3.5$, conductivity $\sigma = 1\,\text{mS/m}$ and thickness $d = 0.3\,\text{m}$. The targets are buried in the second layer which is composed of wet soil characterized by dielectric constant $\varepsilon_r = 8$, conductivity $\sigma = 0.025\,\text{S/m}$ (as shown in Figure 3). The radar operating condition is the same as previous example. The three targets from left to right in Figure 3 are rectangular, cylindrical, and square PEC objects with the designation of Target 1, Target 2, and Target 3 respectively. The spatial characteristics of the three targets are summarized in Table 2.

The investigation domain is a $1.6\,\text{m} \times 1.6\,\text{m}$ square region divided into 100×100 pixels. Figure 4 shows the imaging result of the three targets using the proposed subsurface imaging algorithm, in which the true regions of the three targets are indicated with white dashed circle or rectangles. From this image we find that the three targets are clearly identified and well localized at their true locations. The electromagnetic wave cannot penetrate into PEC objects thus only the upper edges of the objects are imaged. Due to the complexity of the ray tracing technique to deal with multilayered subsurface media, conventional subsurface beamformer could not handle this problem efficiently. Even for a single layer subsurface media it takes about 23.5 s to form the same size image. However, it takes only 0.67 s to form

Table 2. Target spatial characteristics.

	Target Type	Size	Center Position
Target 1	Square	$0.3\,\text{m} \times 0.3\,\text{m}$	$(-0.55\,\text{m}, -0.75\,\text{m})$
Target 2	Cylindrical	radius $= 0.1\,\text{m}$	$(0, -0.6\,\text{m})$
Target 3	Rectangular	$0.4\,\text{m} \times 0.3\,\text{m}$	$(0.5\,\text{m}, -0.85\,\text{m})$

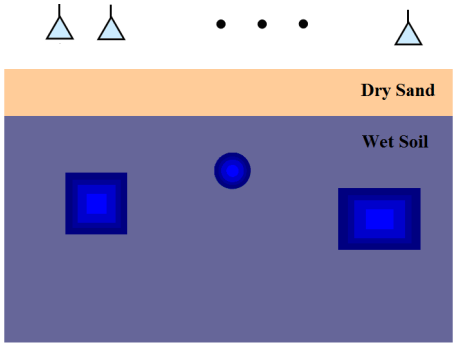

Figure 3. Simulation geometry of multilayer subsurface imaging.

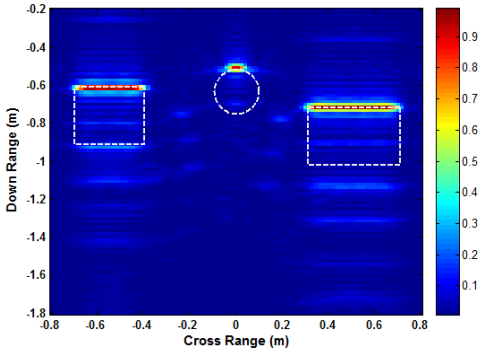

Figure 4. maging of targets under multilayered ground.

the image in Figure 4 using the proposed multilayer subsurface imaging algorithm. Much computation time has been saved in the imaging process due to the employing of FFT in the algorithm. From this result it is clear that the imaging algorithm is very efficient for the imaging of targets buried under multilayer ground in a very short computation time.

3.3. Imaging through Multilayered Building Walls

The capability of EM wave to penetrate through building walls has made through-the-wall radar imaging (TWRI) of increasing interest in both civilian and military applications. Up to present, different TWRI algorithms have been developed for the imaging of targets behind the walls [24, 26–28]. However, most of these algorithms deal with only a single layer wall. In practical applications, we often encounter situations to detect and identify targets behind multilayered walls with composite materials or inside a building with multiple inner walls or walls separated by a hallway [26–28]. This is challenging and is beyond the capability of the existing TWRI algorithms.

In this section, we investigate the imaging of multiple targets behind external and internal walls separated by a hallway, as shown in Figure 5(a). The thickness of the external and internal walls is 0.2 m with relative permittivity $\varepsilon_r = 6$ and conductivity $\sigma = 0.01$ S/m. The width of the hallway between the two walls is 1.2 m. The radar antenna transmits an UWB EM wave covering the frequency range from 1 GHz to 3 GHz and measures the return signal at a distance of 0.3 m from the external wall over a synthetic aperture from -2 m to 2 m. The two targets investigated in this example are two PEC cylinders with a radius of 0.3 m and 0.2 m centred at (-0.7 m, -3.6 m) and (0.8 m, -3.3 m), respectively. The investigation domain is a 2.4 m $\times$ 2 m rectangular region and is divided into 120 $\times$ 100 pixels.

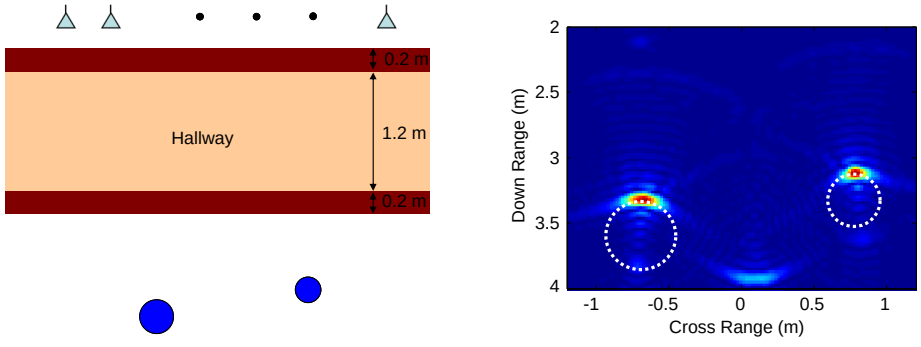

(a) (b)

Figure 5. Two walls separated by a hallway. (a) Simulation configuration. (b) Imaging result.

Figures 5(b) shows the imaging results of the targets using the proposed imaging algorithm, where the correct locations of the targets are indicated with white dashed circles. From Figure 5(b) we find that the two targets are clearly identified and well localized at their correct locations. It is clear from the image that, the propagation effect has been properly taken into account and high quality focused images of the targets can be achieved using the proposed imaging algorithm.

4. CONCLUSION

It is of practical importance and interest in subsurface and urban sensing applications to extend the radar imaging algorithm to the imaging of targets buried under multilayered media. In this paper, a novel tomographic inverse scattering algorithm is proposed for radar imaging through multilayered media with multi-frequency multi-monostatic measurement configuration. The exploding reflection model is employed and then the Green's function is expanded in the spectral domain to facilitate the easy implementation of the imaging algorithm with FFT. Representative examples are presented to show that the imaging algorithm is efficient in the diagnostics of large probed domain and allow real-time processing. This imaging algorithm can be generalized to three-dimensional imaging through multilayered subsurface by incorporation of the layered media dyadic Green's function.

REFERENCES

1. Moustafa, K. and K. F. A. Hussein, "Performance evaluation of separated aperture sensor GPR system for land mine detection," *Progress In Electromagnetics Research*, Vol. 72, 21–37, 2007.
2. Cui, T. J. and W. C. Chew, "Novel diffraction tomographic algorithm for imaging two-dimensional dielectric objects buried under a lossy earth," *IEEE Trans. Geosci. Remote Sens.*, Vol. 38, No. 4, 2033–2041, 2000.
3. Li, L., W. Zhang, and F. Li, "The closed-form solution to the reconstruction of the radiating current for EM inverse scattering," *IEEE Trans. Geosci. Remote Sens.*, Vol. 47, No. 1, 3619–369, 2010.
4. Park, K., S. Park, K. Kim, and K. H. Ko, "Multi-feature based detection of landmines using ground penetrating radar," *Progress In Electromagnetics Research*, Vol. 134, 455–474, 2013.
5. Leuschen, C. J. and P. G. Plumb, "A matched-filter-based reverse-time migration algorithm for ground-penetrating radar data," *IEEE Trans. Geosci. Remote Sens.*, Vol. 39, No. 5, 929–936, 2001.
6. Zhang, W., A. Hoorfar, and C. Thajudeen, "Real time subsurface imaging algorithm for intra-wall characterization," *SPIE conference on Defense, Security, and Sensing*, Vol. 8021, 2011.
7. Liu, X. F., B. Z. Wang, and S. Q. Xiao, "Electromagnetic subsurface detection using subspace signal processing and half-space dyadic green's function," *Progress In Electromagnetics Research*, Vol. 98, 315–331, 2009.
8. Mohammadpoor, M., R. S. A. Raja Abdullah, A. Ismail, and A. F. Abas, "A circular synthetic aperture radar for on-the-ground object detection," *Progress In Electromagnetics Research*, Vol. 122, 269–292, 2012.
9. Chien, W., "Inverse scattering of an un-uniform conductivity scatterer buried in a three-layer structure," *Progress In Electromagnetics Research*, Vol. 82, 1–18, 2008.
10. Abubakar, A., P. M. van den Berg, and J. T. Fokkema, "Linear and nonlinear subsurface inverse scattering algorithms based on the contrast source formulations," *IEEE Antennas and Propagation Society International Symposium*, Vol. 2, 756–760, 2002.
11. Semnani, A. and M. Kamyab, "An enhanced method for inverse scattering problems using fourier series expansion in conjunction with FDTD and PSO," *Progress In Electromagnetics Research*, Vol. 76, 45–64, 2007.
12. Wang, G. L., W. C. Chew, A. A. Aydiner, D. L. Wright, and D. V. Smith, "3D near-to-surface conductivity reconstruction by inversion of VETEM data using the distorted Born iterative method," *Inverse Problems*, Vol. 20, S195–S216, 2004.

13. Cui, T. J., W. C. Chew, A. A. Aydiner, and S. Y. Chen, "Inverse scattering of 2D dielectric objects buried in a lossy earth using the distorted Born iterative method," *IEEE Trans. Geosci. Remote Sensing*, Vol. 39, No. 2, 339–346, 2001.
14. Fen, X., M. Sato, C. Liu, and Y. Zhang, "Profiling the rough surface by migration," *IEEE Trans. Geosci. Remote Sensing Lett.*, Vol. 6, No. 2, 258–262, 2009.
15. Cai, J. and G. A. McMechan, "Ray-based synthesis of bistatic ground-penetrating radar profiles," *Geophysics*, Vol. 60, No. 1, 87–96, 1995.
16. Feng, X. and M. Sato, "Pre-stack migration applied to GPR for landmine detection," *Inverse Problems*, Vol. 20, 99–115, 2004.
17. Counts, T., A. C. Gurbuz, W. R. Scott, J. H. McClellan, and K. Kim, "Multistatic ground-penetrating radar experiments," *IEEE Trans. Geosci. Remote Sensing*, Vol. 45, No. 8, 2544–2553, 2007.
18. Deming, R. and A. J. Devaney, "Diffraction tomography for multi-monostatic ground penetrating radar imaging," *Inverse Problems*, Vol. 13, 29–45, 1997.
19. Hansen, T. B. and P. M. Johansen, "Inversion scheme for monostatic ground penetrating radar that takes into account the planar air-soil interface," *IEEE Trans. Geosci. Remote Sens.*, Vol. 38, No. 1, 496–506, 2001.
20. Crocco, L., F. Soldovieri, T. Millington, and N. J. Cassidy, "Bistatic tomographic GPR imaging for incipient pipeline leakage evaluation," *Progress In Electromagnetics Research*, Vol. 101, 307–321, 2010.
21. Mauriello, P. and D. Patella, "Localization of magnetic sources underground by a probability tomography approach," *Progress In Electromagnetics Research M*, Vol. 3, 27–56, 2008.
22. Witten, A. J., J. E. Molyneux, and J. E. Nyquist, "Ground penetrating radar tomography: Algorithms and case studies," *IEEE Trans. Geosci. Remote Sens.*, Vol. 32, No. 2, 461–467, Mar. 1994.
23. Fallahpour, M., J. T. Case, M. T. Ghasr, and R. Zoughi, "Piecewise and Wiener filter-based SAR techniques for monostatic microwave imaging of layered structures," *IEEE Transactions on Antennas and Propagation*, Vol. 62, No. 1, 282–294, Jan. 2014.
24. Zhang, W. and A. Hoorfar, "Two-dimensional diffraction tomographic algorithm for through-the-wall radar imaging," *Progress In Electromagnetics Research B*, Vol. 31, 205–218, 2011.
25. Lei, W. and J. Liu, "Two-dimensional diffraction tomography algorithm of underground objects located in planar multilayer media," *12nd International Conference on Signal Processing Systems*, Vol. 1, 298–301, 2010.
26. Jia, Y., L. Kong, and X. Yang, "A novel approach to target localization through unknown walls for through-the-wall radar imaging," *Progress In Electromagnetics Research*, Vol. 119, 107–132, 2011.
27. Zhang, W., A. Hoorfar, C. Thajudeen, and F. Ahmad, "Full polarimetric beam-forming algorithm for through-the-wall radar imaging," *Radio Science*, Vol. 46, No. 5, 2011, Doi: 10.1029/2010RS004631.
28. Zhang, W. and A. Hoorfar, "Building layout and interior target imaging with SAR using an efficient beamformer," *IEEE APS/URSI Conference*, 2087–2090, 2011.
29. Li, F., Q. H. Liu, and L. P. Song, "Three-dimensional reconstruction of objects buried in layered media using Born and distorted Born iterative methods," *IEEE Trans. Geosci. Remote Sensing Lett.*, Vol. 1, No. 2, 107–111, 2004.
30. Chew, W. C., *Waves and Fields in Inhomogeneous Media,* Chapter 2, IEEE Press, Piscataway, NJ, 1999.
31. Liu, Y., L. Li, and F. Li, "Imaging of two-dimensional targets buried in a lossy earth with unknown characteristics from multi-frequency and multi-monostatic data," *IET Microwaves, Antennas & Propagation*, Vol. 4, No. 10, 1647–1653, 2010.
32. Zarifi, D., A. Farahbakhsh, A. Abdolali, and M. Soleimani, "Reconstructing constitutive parameters of inhomogeneous planar layered chiral media based on the optimization approach," *Progress In Electromagnetics Research M*, Vol. 29, 29–39, 2013.

33. Spagnolini, U., "Permittivity measurements of multilayered media with monostatic pulse radar," *IEEE Trans. Geosci. Remote Sens.*, Vol. 35, No. 2, 454–463, 1997.
34. Aly, O. and A. S. Omar, "Reconstructing stratified permittivity profiles using super-resolution techniques," *IEEE Trans. Microwave Theory and Tech.*, Vol. 54, No. 1, 492–498, 2006.
35. Leuschen, C. J. and R. G. Plumb, "A matched-filter-based reverse-time migration algorithm for ground-penetrating radar data," *IEEE Trans. Geosci. Remote Sens.*, Vol. 39, No. 5, 929–936, 2001.
36. Li, L., W. Zhang, and F. Li, "Derivation and discussion of the SAR migration algorithm within inverse scattering problem: theoretical analysis," *IEEE Trans. Geosci. Remote Sens.*, Vol. 48, No. 1, 415–422, 2010.